American Mineralogist, Volume 67, pages 76–84, 1982

An ordering model for the commensurate antiphase structure of yoderite

JOHN B. HIGGINS,[1] PAUL H. RIBBE AND YOSHIHARU NAKAJIMA[2]

Department of Geological Sciences
Virginia Polytechnic Institute and State University
Blacksburg, Virginia 24061

Abstract

Yoderite is a high-pressure, high-temperature orthosilicate with similarities to both andalusite and kyanite. Its average structure consists of [010] chains of edge-sharing $[A(1)O_5(OH)]$ octahedra interconnected by isolated $[SiO_4]$ tetrahedra and two edge-sharing trigonal bipyramids of composition $[A(2)O_4(OH)]$ and $[A(3)O_5]$. Using mean *A*–(O,OH) bond lengths and the results of least-squares site refinements for iron, the structural formula may be written $^{vi}[MgAl_3]^{v}[MgAl]^{v}[Al_{.84}Fe^{3+}_{.16}]_2O_2(OH)_2[SiO_4]_4$.

Ordered yoderite has 'e' and 'f' satellite reflections analogous to those in plagioclase feldspars and mullite indicating a commensurate antiphase structure with an *A*-face-centered superlattice of dimensions $a \times 6b \times 2c$, where a, b, c are the cell parameters of the average structure. In our model 3Al + 1Mg are presumed ordered in the edge-sharing $A(1)$ octahedral chains and 1Al + 1Mg in the $A(2)$ trigonal bipyramid which shares an O···OH edge with the $A(1)$ octahedron. Al and Fe^{3+}, which occupy the $A(3)$ teigonal bipyramid in the ratio 5/6 to 1/6, may also be ordered. The $6b$ periodic modulation has conservative antiphase domain boundaries parallel to (010) with a displacement vector of $\frac{1}{2}(2c)$.

Disordered yoderite is produced by heating for 10 hours at 800° C, which destroys the modulation and disorders the iron among the $A(1)$, $A(2)$ and $A(3)$ polyhedra, while leaving the mean *A*–(O,OH) bond lengths essentially unchanged.

Introduction

The orthosilicate mineral yoderite, $Mg_2Al_{5.6}Fe_{0.4}Si_4O_{18}(OH)_2$, has been described from only one locality, Mautia Hill, Tanzania, where it exists as a major phase with quartz, kyanite, and talc (McKie, 1959; McKie and Bradshaw, 1966). Schreyer (1974) calls this assemblage "white-schist;" he believes it formed "under water pressures in excess of some 10 kilobars and at temperatures not higher than 800–840° C." Earlier, Schreyer and Yoder (1968) found that yoderite is stable between 750° and 875° C over a large pressure interval, even somewhat below 10 kbar.

The average structure of $P2_1/m$ yoderite was solved by Fleet and Megaw (1962), who, in their two-dimensional Fourier refinement, deliberately neglected the weak satellite reflections reported by McKie (1959). Described in terms of coordination polyhedra, yoderite consists of chains of edge-sharing $A(1)$ octahedra, $[AO_5(OH)]$, parallel to the b-axis, interconnected by isolated $[SiO_4]$ tetrahedra and two edge-sharing trigonal bipyramids, $A(2)$ and $A(3)$ of composition $[AO_4(OH)]$ and $[AO_5]$, where A = Al,Mg,Fe^{3+} (Figs. 1 and 2). Thus a simplified structural formula of yoderite can be written ^{vi}(Mg, Al,Fe^{3+})$_4{}^{v}$(Mg,Al,Fe^{3+})$_4O_2(OH)_2[SiO_4]_4$. This is essentially the same as the andalusite formula with 2Mg + 2(OH) → 2Al + 2O. Based on recognition by McKie (1959) that the lattice parameters of yoderite are very similar to those of kyanite, Fleet and Megaw (1962; see their Fig. 3) noted that the edge-sharing octahedral chains parallel to c in kyanite are linked by other $[AlO_6]$ octahedra instead of $[AO_5]$ trigonal bipyramids, as they are in yoderite. Yoderite and kyanite are frequently intergrown, and their topotaxy results from their structural similarity: $\alpha_{yo} \| b_{ky}$; $b_{yo} \| c_{ky}$; $c_{yo} \angle \alpha_{ky} \simeq 11°$.

As suggested by the structural formula, yoderite, with oxygen packing index P = 0.058 oxygens/Å^3, and andalusite (P = 0.061 oxygens/Å^3) are in many

[1]Present address: Mobil Research & Development Corp., P.O. Box 900, Dallas, Texas 75221.

[2]Present address: Department of Earth & Space Sciences, State University of New York, Stony Brook, New York 11794.

0003–004X/82/0102–0076$02.00

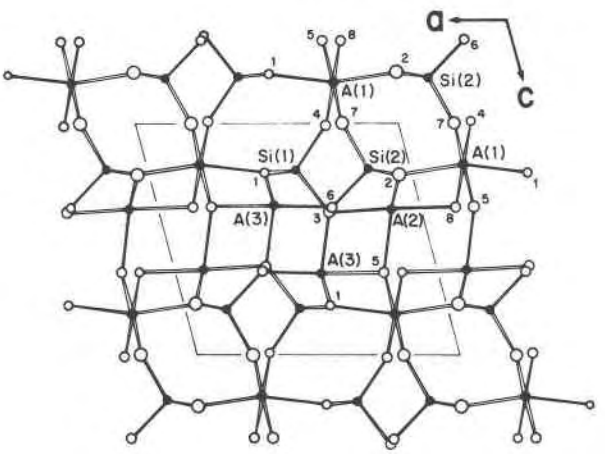

Fig. 1. A partial projection of the average structure of yoderite onto the *ac* plane. Oxygen atoms (open circles) are labelled with numbers only: O(8) is presumed to be the (OH) anion (Fleet and Megaw, 1962). The *A*(1) cations are octahedrally coordinated, *A*(2) and *A*(3) are 5-coordinated, and Si(1) and Si(2) are 4-coordinated. See Figure 2.

ways more analogous than are yoderite and the much more dense kyanite (P = 0.068 oxygens/Å^3). They have similar pairs of edge-sharing [AX_5] trigonal bipyramids of "composition" [A_2X_8], although in yoderite these link only two chains of edge-sharing [AX_6] octahedra together whereas in andalusite they link four such chains (*cf.* Fig. 4 of Vaughn and Weidner, 1978, p. 141).

McKie (1959) observed satellite reflections in X-ray photographs of yoderite indicative of a superstructure or modulated structure normal to (010). Because the reflections weakened in intensity and finally disappeared upon heating, McKie suggested that the superstructure may be related to some (undesignated) scheme of Mg/Al ordering in the octahedral sites. In order to investigate this possibility we have completed two room-temperature structure refinements of yoderite. The first was undertaken on an unheated crystal exhibiting satellite reflections: we call this *ordered* yoderite for reasons which will become evident. The satellite reflections were too few and weak to be useful in refining the large supercell, so only the *average* structure was refined. Another refinement was undertaken on a heated crystal—*disordered* yoderite—which has no satellite reflections. In addition a study by high-resolution transmission electron microscopy (HRTEM) of the ordered phase was made in an attempt to discern the nature of the superstructure. Preliminary reports of this work were presented by Higgins and Ribbe (1977) and Ribbe *et al.* (1981).

Experimental details

Sample description

A specimen of purple yoderite (No. 137854) from Mautia Hill, Tanzania was provided for our investigation by Mr. John S. White of the U.S. Museum of Natural History. This is the only known locality for yoderite, but it occurs in two distinct colors, green and purple. Abu-Eid *et al.* (1978) examined these using Mössbauer and polarized optical absorption spectroscopy and found that both varieties had an $Fe^{2+}/(Fe^{2+} + Fe^{3+})$ ratio of ~0.05, but that the purple specimen contained 0.01 Mn^{2+} and 0.07 Mn^{3+} atoms per unit cell, whereas the green variety contained <0.001 Mn^{2+} and no discernable Mn^{3+}. Our microprobe analyses of purple yoderite are in substantial agreement with theirs (to within 0.04 atoms for all elements); we have used the following stoichiometry: $Mg_2Al_{5.6}Fe^{3+}_{0.4}O_2(OH)_2[SiO_4]_4$. The lattice parameters and other pertinent crystal data are listed in Table 1.

Crystal structure refinements

Two small cleavage fragments from a larger crystal of yoderite were selected for structure refinement. One of these was heated in a platinum liner at 800° C in an argon atmosphere for 15 days, and then it was quenched in argon. Examination of a long-exposure (0*kl*) precession photograph of the heated grain showed no satellite reflections of the sort evident in the unheated crystal. Prior to intensity data collection the absence of satellites in the heated grain was confirmed by searching in vain

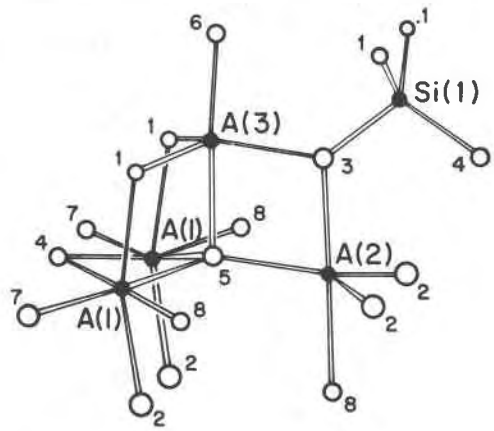

Fig. 2. A partial polyhedral drawing of yoderite showing the linkage of the *A*(1) octahedra, *A*(2) and *A*(3) trigonal bipyramids and one of the Si tetrahedra. The O,OH anions are identified with small numbers (*cf.* Fig. 1).

Table 1. Summary of crystal data and optical properties for Mautia Hill yoderites

Lattice parameters (purple crystal; this study)

	Ordered, 20°C	Ordered, 800°C	Disordered, 20°C
a	8.022(2) Å	8.073(3) Å	8.027(2) Å
b	5.816(1)	5.848(2)	5.805(1)
c	7.250(2)	7.277(3)	7.252(2)
β	104.9(1)°	104.9(1)°	104.9(1)°

Density, ordered specimen: 3.38 gcm^{-3}

Space group, all crystals: $P2_1/m$ (see text for comment)

Linear absorption coefficient for Mo$K\alpha$ radiation: 14.8 cm^{-1}

Optical properties (20°C)

	α	β	γ	$2V_\gamma$	$Z\hat{}c$
Purple*	1.689(2)	1.691(2)	1.715(2)	25°	7°
Green**	1.691(3)	1.693(3)	1.712(3)	30°	-

Pleochroism, unheated crystals

	α	β	γ
Purple*	Prussian blue	Indigo	Olive green
Green**	Green	Pale yellow	Yellow

Cleavage: {001} Parting*: [001] moderately good, {100} poor

* Data by McKie (1959) from a characteristically purple crystal with ~0.03 Mn atoms per formula unit, whose color is ascribed to the chromophore group Mn^{3+}–O–Mn^{2+} (McKie and Bradshaw, 1966). Abu-Eid *et al.* (1978) ascribe the purple color to Mn^{2+}–Mn^{3+} charge transfer. Fe^{3+} is the predominant iron species: Fe^{3+}/total iron = 0.95.

** Data by McKie and Bradshaw (1966). Both they and Abu-Eid *et al.* (1978) ascribe the green color to Fe^{3+}–Fe^{2+} charge transfer. See text for further discussion.

with the automated diffractometer for two *e*-type reflections which were the most intense in the unheated crystal. Heating produced no changes in color, although $2V_\gamma$ increased from ~25° in the unheated crystal to ~60°.

Identical data sets from both crystals were collected on a Picker FACS-1 system. The resultant intensities were corrected for background, Lorentz-polarization and absorption effects. Data reduction, refinement, and geometry calculations were carried out using locally modified versions of DATALIB, DATASORT, RFINE IV and ORFEE 3 (World List of Crystallographic Computer Programs, 3rd edition and supplements). The data reduction and refinement techniques are listed in Table 2. Refinement of both X-ray data sets was initiated using positional and thermal parameters of Fleet and Megaw (1962). X-ray scattering factors were taken from Volume III of *International Tables for X-ray Crystallography*. Non-tetrahedral *A*-site occupancies were refined subject to the constraints of the structural formula (Table 1) employing the method of derivative modification and parameter restoration developed by Finger (1969). Positional and isotropic thermal parameters and site occupancies of both data sets converged within four cycles of full-matrix, least-squares refinement and are listed in Table 3. Interatomic distances and angles are given in Table 4.

Results of both refinements confirmed the original structure solution of Fleet and Megaw (1962); however, attempts to refine the x and z parameters of the hydrogen atom presumably bonded to O(8) proved unsuccessful. Comparison of the two refinements of this study and the two-dimensional Fourier refinement of Fleet and Megaw (1962) show significant differences in some individual Si–O and

Table 2. Data reduction and refinement statistics for unheated (*ordered*) and heated (*disordered*) yoderite

	Unheated	Heated
Number of reflections measured	1631	2282
Number of independent reflections	1097	1097
Agreement factor among averaged reflections	0.04	0.02
Number of independent reflections with $I > 2\sigma$	499	499
Weighted R factor, all data $wR = [\Sigma w (\lvert F_o \rvert - \lvert F_c \rvert)^2 / \Sigma w F_o^2]^{\frac{1}{2}}$	0.056	0.050
R factor, all data $R = \Sigma \lvert \lvert F_o \rvert - \lvert F_c \rvert \rvert / \Sigma \lvert F_o \rvert$	0.060	0.039
Weighted R, observed data	0.054	0.049
R, observed data	0.051	0.035
Standard deviation of unit weight observation	2.70	3.13

Table 3. Atomic coordinates, temperature factors and metal site occupancies for unheated and heated (italics) yoderite

Atom	Iron content	x	y	z	$B(A^2)$
Si(1)		0637(3)*	2500	7984(4)	46(4)
		0634(2)	*2500*	*7987(2)*	*39(3)*
Si(2)		3396(3)	7500	8024(4)	61(4)
		3393(2)	*7500*	*8014(2)*	*56(3)*
A(1)	0.01	2952(2)	0051(3)	1776(3)	56(4)
	0.06	*2948(2)*	*0049(2)*	*1780(2)*	*58(3)*
A(2)	0.02	3888(4)	2500	6301(4)	72(6)
	0.06	*3889(2)*	*2500*	*6299(3)*	*59(4)*
A(3)	0.16	0557(3)	2500	3539(4)	75(4)
	0.07	*0559(2)*	*2500*	*3543(2)*	*47(3)*
O(1)		0573(5)	9801(7)	2147(6)	69(6)
		0562(4)	*9804(4)*	*2156(4)*	*60(4)*
O(2)		4525(6)	9760(8)	7812(7)	133(7)
		4532(4)	*9764(5)*	*7785(5)*	*114(5)*
O(3)		1478(8)	2500	6145(10)	91(9)
		1489(6)	*2500*	*6166(7)*	*80(6)*
O(4)		2206(8)	2500	9928(9)	72(8)
		2207(6)	*2500*	*9930(6)*	*74(6)*
O(5)		2979(9)	2500	3615(10)	93(9)
		2995(6)	*2500*	*3622(7)*	*78(6)*
O(6)		1652(8)	7500	6322(10)	81(9)
		1645(6)	*7500*	*6299(7)*	*72(6)*
O(7)		2830(9)	7500	0045(10)	106(9)
		2842(6)	*7500*	*0040(6)*	*93(6)*
O(8)		3597(8)	7500	3643(10)	116(10)
		3623(6)	*7500*	*3631(7)*	*104(8)*

* Positional parameters × 10^4, thermal parameters × 10^2. Numbers in parentheses represent e.s.d.'s in terms of the least significant figure to the left.

Table 4. Yoderite interatomic distances (Å) and angles(°)

	unheated	heated		unheated	heated
Tetrahedra					
Si(1)-O(1)	1.642(4)	1.636(3)	Si(2)-O(2)	1.626(5)	1.635(3)
O(1)	1.642(4)	1.636(3)	O(2)	1.626(5)	1.635(3)
O(3)	1.642(8)	1.637(5)	O(6)	1.610(6)	1.617(5)
O(4)	1.630(6)	1.632(4)	O(7)	1.642(8)	1.639(5)
mean	1.639	1.635		1.626	1.632
Octahedron					
A(1)-O(1)	2.000(5)	2.007(4)			
O(2)	1.972(5)	1.967(4)			
O(4)	1.942(5)	1.943(3)			
O(5)	1.947(6)	1.947(4)			
O(7)	1.929(5)	1.934(3)			
O(8)	1.985(5)	1.979(3)			
mean	1.963	1.963			
Trigonal bipyramids					
A(2)-O(2)	1.927(5)	1.916(3)	*A*(3)-O(1)	1.868(5)	1.863(3)
O(2)	1.927(5)	1.916(3)	O(1)	1.868(5)	1.863(3)
O(3)	1.907(7)	1.903(2)	O(3)	1.843(7)	1.856(5)
O(5)	1.896(7)	1.888(5)	O(5)	1.929(7)	1.940(5)
O(8)	2.008(7)	1.983(5)	O(6)	1.801(7)	1.801(5)
mean	1.933	1.921		1.862	1.865
O-T-O Angles					
Si(1) tetrahedron			**Si(2) tetrahedron**		
O(4)-O(1)	111.3(2)	111.4(1)	O(6)-O(2)	108.8(2)	108.6(2)
O(3)	108.4(4)	107.8(2)	O(7)	107.4(4)	107.9(3)
O(1)-O(1)	109.2(3)	110.0(2)	O(2)-O(2)	107.9(4)	107.2(2)
O(3)	108.3(2)	108.0(1)	O(7)	111.9(2)	112.2(2)
O-*A*-O Angles					
***A*(1) octahedron**			***A*(2) trigonal bipyramid**		
O(7)-O(4)	99.2(2)	99.1(1)	O(5)-O(3)	79.8(3)	80.6(2)
O(5)	176.0(3)	176.7(2)	O(2)	124.0(2)	123.6(1)
O(2)	91.1(3)	91.0(2)	O(8)	98.0(3)	98.0(2)
O(8)	80.2(2)	80.0(2)	O(3)-O(2)	98.6(2)	98.7(1)
O(1)	98.1(3)	98.7(2)	O(8)	177.8(3)	178.6(2)
O(4)-O(5)	83.3(2)	83.4(2)	O(2)-O(2)	111.6(3)	112.2(2)
O(2)	100.7(3)	100.9(2)	O(8)	82.5(2)	82.1(1)
O(8)	177.2(3)	178.0(2)	***A*(3) trigonal bipyramid**		
O(1)	90.6(2)	90.7(2)			
O(5)-O(2)	91.4(3)	90.7(2)	O(6)-O(3)	94.8(3)	94.4(2)
O(8)	97.2(2)	97.4(2)	O(1)	100.0(2)	99.9(1)
O(1)	78.7(3)	79.0(2)	O(5)	175.3(3)	174.8(2)
O(2)-O(8)	82.0(2)	80.9(2)	O(3)-O(1)	119.8(1)	119.8(1)
O(1)	164.1(2)	163.5(2)	O(5)	80.5(3)	80.4(2)
O(8)-O(1)	86.8(2)	87.6(2)	O(1)-O(1)	114.3(3)	114.7(2)
			O(5)	82.4(1)	82.8(1)

A–O bond distances (Table 4); however, mean polyhedral bond distances of the three refinements are remarkably similar, as indicated below:

		This study	
	Fleet & Megaw	*Unheated*	*Heated*
⟨Si(1)–O⟩	1.638Å	1.639Å	1.635Å
⟨Si(2)–O⟩	1.631	1.626	1.632
⟨*A*(1)–O,OH⟩	1.966	1.963	1.963
⟨*A*(2)–O,OH⟩	1.935	1.933	1.921
⟨*A*(3)–O⟩	1.870	1.862	1.865

Comparison of positional parameters of the two refinements of this study is facilitated by use of half-normal probability plot analysis (see Higgins and Ribbe, 1979). This technique is useful in detecting differences between two parameter sets and in estimating the reliability of their assigned standard deviations. The linearity of the plot in Figure 3 and its near-zero intercept indicate the absence of significant differences in positional parameters resulting from systematic errors; however, the deviation of the slope from unity indicates that the pooled standard deviations have been underestimated by a factor of about 1.3.

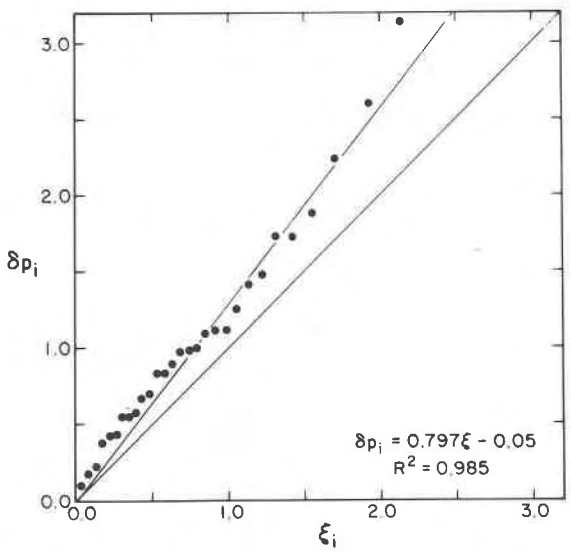

Fig. 3. A half-normal probability plot relating δp_i and ξ_i for the two crystal structure refinements of yoderite. See the text and Abrahams (1972, 1974) for interpretation.

In order to test the possibility that the superstructure in yoderite resulted from cation ordering, site refinements of the non-tetrahedral cations were attempted. Because of the almost identical X-ray scattering powers of Mg and Al, site refinements of these elements were unsuccessful, and any conclusions as to the relative distribution of Al and Mg among the *A* polyhedra must be deduced from mean *A*–O bond lengths. However, the considerable difference between the scattering curves for Fe and (Mg,Al) permitted us to refine the iron contents of the polyhedra (Table 3). These refinements indicate that in heated yoderite the ~0.4 Fe atoms per unit cell are disordered among the three non-tetrahedral metal sites while in the unheated yoderite iron is ordered primarily into the *A*(3) trigonal bipyramid (0.16 atoms) with 0.01 and 0.02 iron atoms in the *A*(1) octahedron and the *A*(2) trigonal bipyramid, respectively.

X-ray and electron diffraction observations

A precession camera was used to record X-ray diffraction patterns of the *hk*0, *hk*1, 0*kl* and 1*kl* levels of the reciprocal lattice. The observations of McKie (1959) were confirmed, but the intensities of the satellite reflections were very weak. These

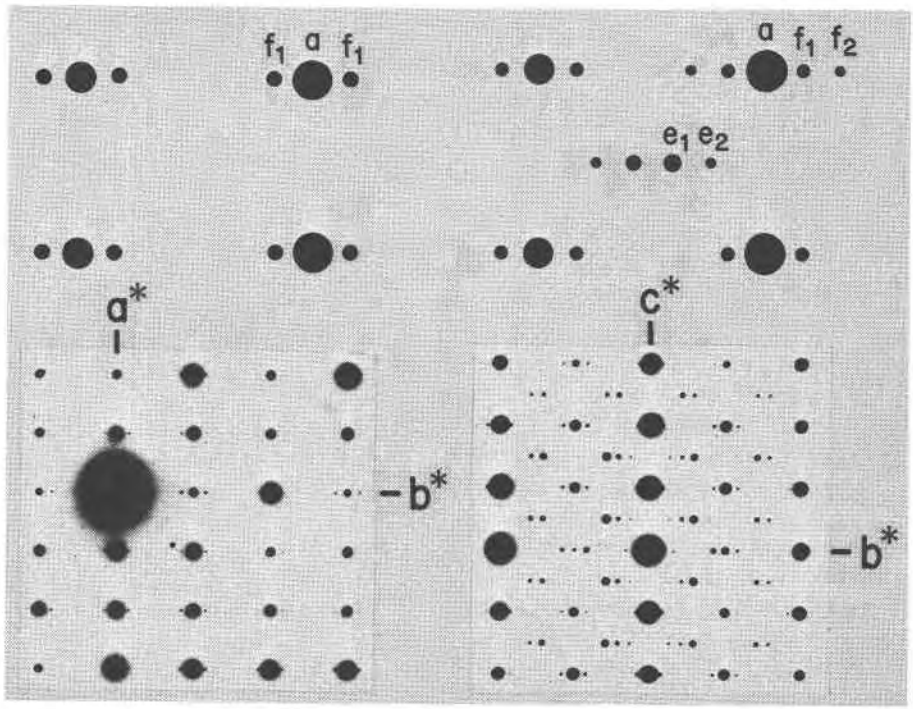

Fig. 4. a^*b^* and b^*c^* electron diffraction patterns of ordered (unheated) yoderite with exploded reciprocal cells (above) labelled according to conventions established by Bown and Gay (1958) for the antiphase structures of intermediate plagioclases. 'e_1' and 'e_2' represent first- and third-order satellites disposed along b^* about the absent reflection with indices $k + ½, l + ½$; 'f_1' and 'f_2' represent second- and fourth-order satellites to the 'a' sublattice reflections.

reflections are reminiscent of the 'e'- and 'f'-type satellites observed in plagioclase feldspars of composition $Na_{1-z}Ca_zAl_{1+z}Si_{3-z}O_8$, where $0.25 < z < 0.75$ (Bown and Gay, 1958), and mullites, $Al_2(Al_{2+2x}Si_{2-2x})O_{10-x}$, where $0.17 < x < 0.59$ (Cameron, 1977; Nakajima and Ribbe, 1981).

These reflections are strikingly enhanced in electron diffraction patterns (Fig. 4), and careful measurement indicates that the periodicity of the commensurate antiphase domain structure along the b^* direction is exactly $6b$. This is confirmed by lattice images made from carbon-coated, crushed grains dispersed on holey carbon in a JEOL 200CX transmission electron microscope at the Department of Earth and Space Sciences, State University of New York, Stony Brook, New York. The $0kl$ image is reproduced in Figure 5.

To be consistent with symbols used for satellite reflections in intermediate plagioclases and mullite, the 'e' reflections (Fig. 4) are labeled 'e_1' and 'e_2,' corresponding to first- and third-order reflections, and the 'f' reflections are labeled 'f_1' and 'f_2,' corresponding to second- and fourth-order satellites. The extinctions observed are proof that the average structure related across the antiphase domain boundaries (APB's) is pseudo-*A*-face-centered: maxima which would appear at $k + ½, l + ½$ in the diffraction pattern of a truly *A*-centered cell are absent in the $0kl$ net (Fig. 4b) and have been replaced by 'e' satellites which are symmetrically disposed about that point in the $0kl$ net. Their attendant 'f' satellites are symmetrically disposed about the hkl diffraction maxima which, if the cell were truly *A*-centered, would have only k- and l-even indices in the $0kl$ net. We have chosen *not* to reindex the yoderite pattern to accommodate this pseudo-*A*-centering, so the satellite reflections observed have indices as follows:

$$\text{'e}_1\text{'} \quad h,\ k+\frac{1}{2}\pm\frac{1}{12},\ l\pm\frac{1}{2} \qquad \text{'f}_1\text{'} \quad h,\ k\pm\frac{2}{12},\ l$$

$$\text{'e}_2\text{'} \quad h,\ k+\frac{1}{2}\pm\frac{3}{12},\ l\pm\frac{1}{2} \qquad \text{'f}_2\text{'} \quad h,\ k\pm\frac{4}{12},\ l$$

The unit repeat of the yoderite supercell is a, $6b$, $2c$ (where a, b, c are the cell dimensions of the average structure), and these translationally equivalent

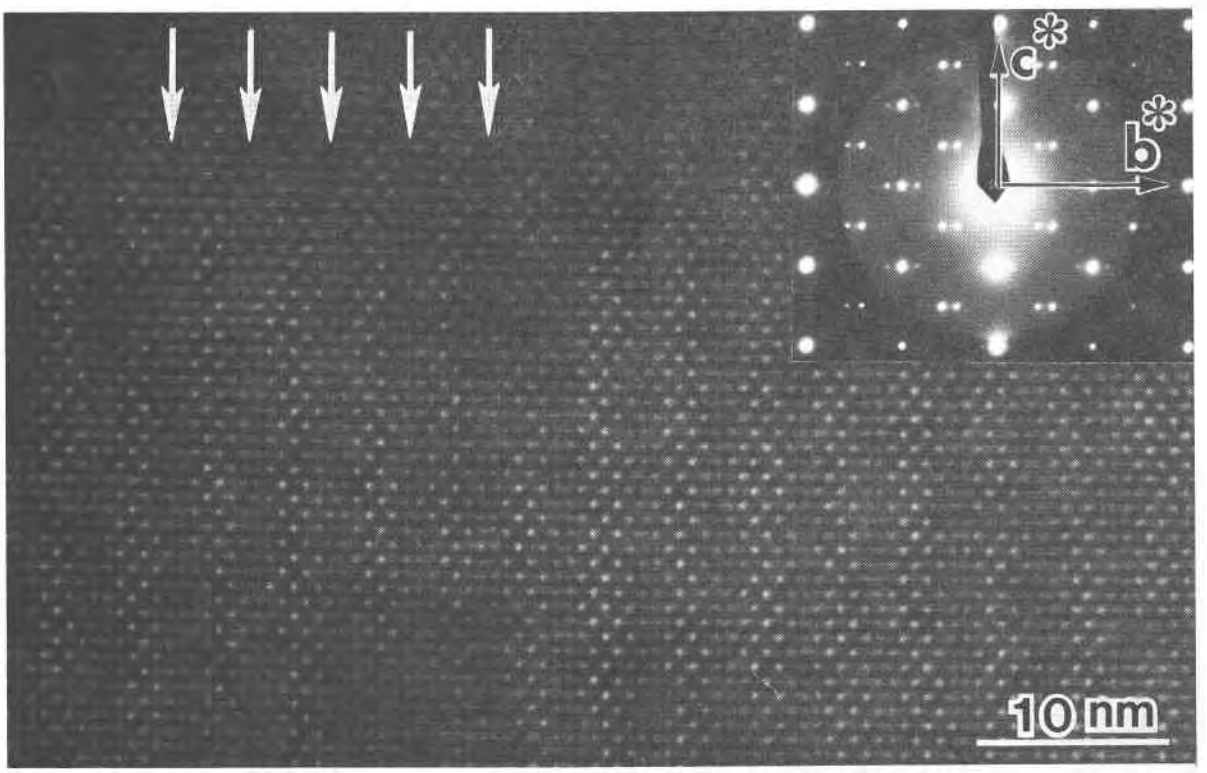

Fig. 5. A multiple-beam high-resolution TEM image of the commensurate antiphase structure of yoderite taken at 200 kV with [100] parallel to the electron beam. Compare with Figs. 6 and 8.

units are oriented in an *A*-centered array, as sketched in Figure 6.[3]

McKie (1959) reported that with heating at 800° C the satellite reflections remained sharp and did not migrate, but gradually lost intensity. We monitored the most intense 'e' reflection on the Picker FACS-1 diffractometer at 600° and 700° C and found no change in relatively short times of heating, but—in confirmation of McKie's observation—we found that at 800° C the 'e' intensity decreased with time as shown in Figure 7, reaching zero after ~10 hours.

Discussion of the antiphase structure

Summary of data

Inasmuch as Fleet and Megaw (1962) successfully solved the average structure of unheated yoderite and obtained, using 2-D Fourier methods, a refinement not significantly different from our 3-D least-squares results, we are left with the task of deducing the possible causes of the modulated structure of 'ordered' yoderite, knowing only that (1) upon heating at 800° C the satellite reflections (and thus the periodic modulation responsible for them) weaken and disappear without becoming diffuse; (2)

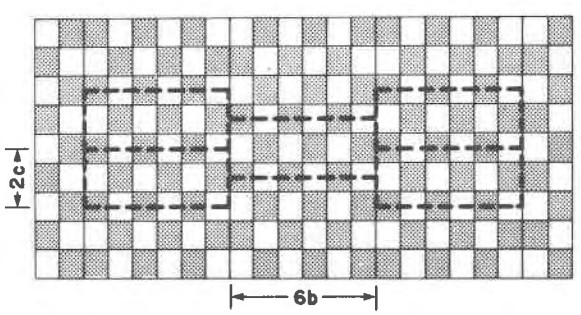

Fig. 6. A schematic representation of the distribution in the plane normal to [100] of the two types of subcells in the antiphase structure of yoderite. Compare with Figs. 5 and 8. Note the *A*-centered array of supercells with dimensions $6b \times 2c$.

[3]See Korekawa (1967), Jamieson *et al.* (1969) and Böhm (1975, 1976) for diffraction theory of satellite reflections, Smith (1974, Ch. 5) for application to plagioclases and Nakajima and Ribbe (1981) for application to mullite.

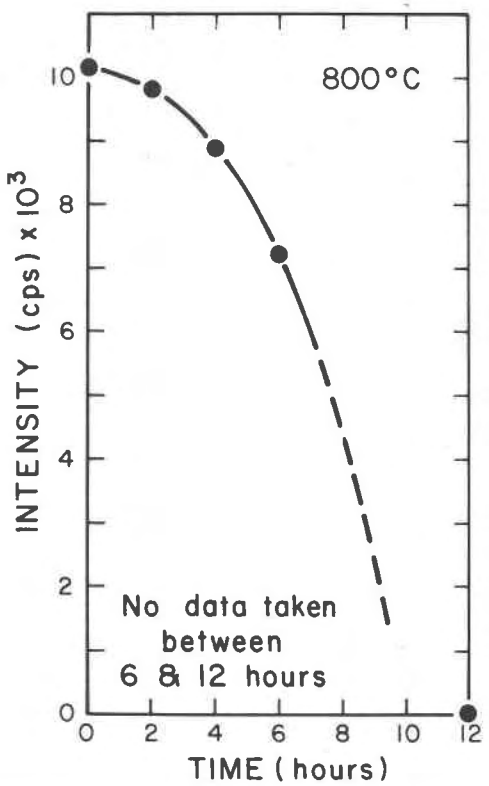

Fig. 7. The intensity of an 'e' satellite reflection in yoderite monitored for 12 hours at 800° C.

iron has an ordered distribution in the unheated specimen and a disordered distribution in the heated one; and (3) the mean *A*–O bond lengths for the *A*(1) octahedra and *A*(2) and *A*(3) trigonal bipyramids remain basically unchanged after heating.

A model of the superstructure

McKie (1959) suggested that the superstructure of yoderite might be due to Mg,Al ordering in the octahedral sites, and this may indeed be the case. But inasmuch as we were unable to refine the Mg,Al distribution in the $[AX_6]$ and $[AX_5]$ polyhedra with X-ray methods, our site assignment for the *average* structure of ordered yoderite must be based on interpretations of the mean *A*(1)–, *A*(2)– and *A*(3)–O bond lengths. Least-squares site refinement indicated that 0.16 Fe atoms occupy each of the two equivalent *A*(3) sites, but to find meaningful reference points for determining Mg,Al distributions, data from structurally somewhat similar aluminum silicate minerals were used (Winter and Ghose, 1979).

The [A(3)O₅] polyhedron. As mentioned in the introduction, there are many structural similarities between yoderite and andalusite, $^{vi}Al^{v}AlO[SiO_4]$. In andalusite there is an $[AlO_5]$ polyhedron which has a mean ^{v}Al–O bond length of 1.836Å, but in our ordered yoderite the *A*(3) trigonal bipyramid contains 0.16 Fe + 0.84 Al. In order to estimate the effect of Fe^{3+} substitution on the mean *A*(3)–O bond length, we used the difference between the Shannon (1976) ionic radii for Al^{3+} (r = 0.48Å) and Fe^{3+} in 5-fold coordination (the latter value was interpolated to be r = 0.705Å). The predicted mean bond length is 1.87Å, in satisfactory agreement with the observed value of 1.862. It should not escape notice that the supercell of yoderite has a 6*b* repeat, and the fractions of Fe and Al occupying *A*(3) are close to ⅙ and ⅚, respectively.

The [A(2)O₄(OH)] polyhedron. Using the same approach as for *A*(3) and a Shannon (1976) radius for ^{v}Mg of 0.66Å, the mean ^{v}Mg–(O,OH) distance is estimated to be 2.016Å. If one of the two equivalent *A*(2) sites in the unit cell of the average structure were occupied by Al and one by Mg, the mean bond length predicted, based on 0.5 Mg + 0.5 Al occupancy, would be 1.926Å, in excellent agreement with the observed ⟨*A*(2)–O,OH⟩ value of 1.933Å. The minute quantity of Fe^{3+} assigned to this site (Table 3) was ignored in this calculation.

The [A(1)O₅(OH)] polyhedron. The octahedron is more difficult to interpret because the corresponding octahedron in andalusite has ⟨Al–O⟩ = 1.935Å, whereas in kyanite the mean Al–O distance for the 4 octahedra is 1.907Å. Using a compromise value—the average of these two—for mean ^{vi}Al–O and the difference in the Shannon (1976) ionic radii for six-coordinated Al^{3+} and Mg^{2+}, a very reasonable mean ^{vi}Mg–O distance of 2.106Å is thereby estimated. The chemical constraints of previous estimates of site occupancies leave one Mg and three Al atoms to be distributed among the four equivalent *A*(1) sites in average yoderite. Since ¼⟨^{vi}Mg–O⟩ + ¾⟨^{vi}Al–O⟩ = 1.967Å—a value embarrassingly close to the observed 1.963Å, we may assume this distribution is reasonable, particularly because it conveniently provides for an ordered model of Mg,Al distribution between the *A*(2) and *A*(1) sites.

The average-structure formula for ordered yoderite. The cation distribution proposed above leads to the following structural formula for the average unit cell of ordered yoderite: $^{vi}[MgAl_3]^{v}[MgAl]^{v}[Al_{.84}Fe^{3+}_{.16}]_2O_2(OH)_2[SiO_4]_4$.

A proposed Mg,Al,Fe ordering scheme. Figure 8 is a projection onto the (100) plane of the distribution of non-tetrahedral cation sites whose associat-

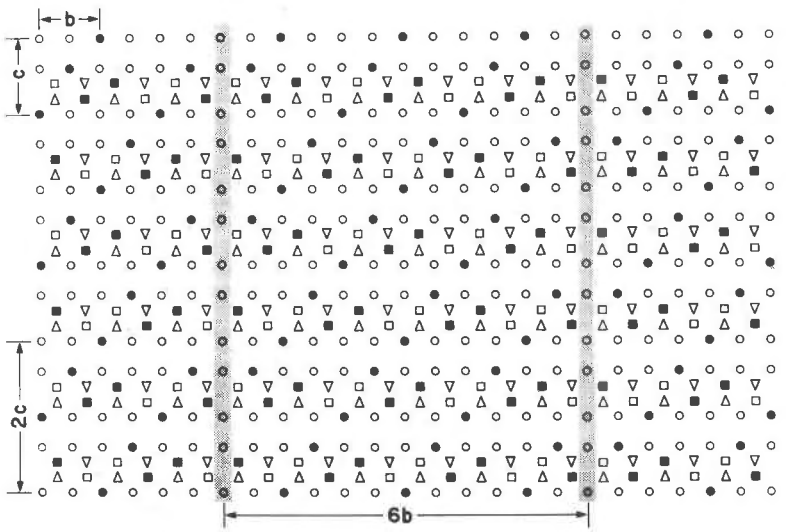

Fig. 8. A schematic representation of the distribution of Mg (filled symbols) and Al (open symbols) in the $A(1)$ octahedra (circles) that comprise the edge-sharing chains parallel to [010], in the $A(2)$ trigonal bipyramids (squares) that share an O···OH edge with $A(1)$ octahedra, and in the $A(3)$ trigonal bipyramids (triangles) that share an edge with $A(2)$ polyhedra (*cf.* Fig. 2) and contain most of the iron in ordered yoderite. The conservative APB's are represented by shaded strips normal to [010]; displacement vectors are $\frac{1}{2}(2c)$. See text for discussion.

ed polyhedra share edges as indicated in Figure 2. One of every four $A(1)$ sites is a black dot indicating Mg occupancy; the open circles contain Al. Every other $A(2)$ site (squares) is black, also to indicate Mg, but none of the $A(3)$ sites (triangles) are black, indicating probable absence of Mg from $A(3)$. Because almost exactly one-sixth of the $A(3)$ sites contain Fe and five-sixths contain Al, one is tempted to assign the iron atoms to those sites near the antiphase boundary, as indicated by the shaded strips at $6b$ intervals. Upon casual consideration, one might protest that the rapidity with which the structure (*i.e.*, the iron) disorders at 800° C argues against so wide-spread a distribution of the only cation which is known to migrate in significant amounts from one polyhedron to the other two. But in fact the iron need disorder only locally to accomplish a random distribution among $A(1)$, $A(2)$ and $A(3)$ sites of the *average* cell. Perhaps a more cogent argument is the lack of any diffraction contrast that might be expected if iron were ordered in a completely regular array.

Inasmuch as the heating which is sufficient to destroy the antiphase domains does not significantly change any of the mean A-polyhedral bond lengths, it may be assumed that most of the other disordering that occurs is *among* $A(1)$ octahedra or *between* $A(1)$ and $A(2)$ polyhedra whose shared edge, according to Fleet and Megaw (1962), involves the only (OH) anion in the structure. Exchange across this O···OH edge is constrained to be balanced, *i.e.*, one-for-one Mg for Al. The $A(3)$ site loses 0.1 Fe^{3+}, which is a relatively large cation, and possibly small amounts of Al, but probably gains relatively large Mg to compensate for the loss. It is, of course, conceivable that further heating at 800° C or heating at somewhat higher temperatures would produce a more pronounced disordering of Al and Mg. McKie (1959) reports decomposition of yoderite to mullite and an unidentified phase after heating at 950° C.

Note that this model (Fig. 8) of the ordered structure provides for a doubling of the c dimension of the cell of the average structure (represented by a single rectangle), and that after every sixth repeat along b the otherwise perfectly ordered structure is displaced $\frac{1}{2}(2c)$, as observed in the lattice image (Fig. 5). Furthermore, as required by satellite reflection extinctions, the superstructure as an A-centered arrangement (*cf.* Figs. 5 and 6) and all the atoms within the $a \times 6b \times 2c$ supercell are related by $(b + c)$, forming an A-centered sublattice of dimensions $2b \times 2c$. The antiphase shift across the APB is $\frac{1}{2}(2c)$, and since the displacement vector is parallel to the APB, no compositional change is introduced by the boundary. Anything other than this sort of *conservative* APB would disrupt the stoichiometry significantly.

Apart from the possibility of a short-range ordering of iron on one of every six $A(3)$ sites, no other

cause of the 6*b* modulation is immediately evident. As long as the APB's are conservative, there is no compelling reason (except Fe^{3+} ordering) why the modulation could not be 2*b*, 4*b* or any even multiple of the *b* dimension of the average cell. The antiphase boundary region (shaded in Fig. 8) was arbitrarily selected; cation occupancies are not specified, because, although one expects a ratio of 3Al:1Mg in those *A*(1) octahedra, the structural adjustment occurring there (or wherever the boundaries really are) makes speculation unproductive. It is noteworthy that, even in the small sample of the lattice image shown in Figure 5, the boundary region is seen not to be entirely uniform. In fact other images show it to be occasionally somewhat curved and irregular.

The ordering scheme suggested herein makes use of the Mg,Al,Fe distribution suggested by mean *A*–O bond lengths and least-squares site refinement of Fe, but other configurations are certainly conceivable. We offer this as a reasonable possibility. Our attempts to collect X-ray data from the 'e' satellites were disappointing due to their very low intensities. A neutron diffraction refinement of the average structure would produce more definitive Mg,Al,Fe distributions, but might not shed additional light on the real nature of the ordered supercell.

Acknowledgments

This work was supported in large measure by National Science Foundation grant EAR77-23114 to P. H. Ribbe and G. V. Gibbs. Dr. F. K. Ross and Dr. G. L. Nord, Jr. are gratefully acknowledged for their assistance with X-ray diffraction and electron diffraction experiments, respectively.

References

Abrahams, S. C. (1972) Systematic error differences between two refined sets of position coordinates for $Na_3PO_3CO_2 \cdot 6H_2O$. Acta Crystallographica, B28, 2886–2887.

Abrahams, S. C. (1974) The reliability of crystallographic structural information. Acta Crystallographica, B30, 261–268.

Abu-Eid, R. M., Langer, K., and Seifert, F. (1978) Optical absorption and Mössbauer spectra of purple and green yoderite, a kyanite-related mineral. Physics and Chemistry of Minerals, 3, 271–289.

Böhm, H. (1975) Interpretation of X-ray scattering patterns due to periodic structural fluctuations. I. The case of transverse modulation of positional parameters in primitive lattices. Acta Crystallographica, A31, 622–628.

Böhm, H. (1976) Interpretation of X-ray patterns due to modulation of positional parameters and of scattering density. Zeitschrift für Kristallographie, 143, 56–66.

Bown, M. G., and Gay, P. (1958) The reciprocal lattice geometry of the plagioclase feldspar structure. Zeitschrift für Kristallographie, 111, 1–14.

Cameron, W. E. (1977) Mullite: a substituted alumina. American Mineralogist, 62, 747–755.

Finger, L. W. (1969) Determination of cation distribution by least-squares refinement of single crystal X-ray data. Carnegie Institution of Washington Year Book, 67, 211–217.

Fleet, S. G., and Megaw, H. D. (1962) The crystal structure of yoderite. Acta Crystallographica, 15, 721–728.

Higgins, J. B., and Ribbe, P. H. (1977) The crystal structure and domain texture of yoderite. Geological Society of America Abstracts with Programs, 9, 1015.

Higgins, J. B., and Ribbe, P. H. (1979) Sapphirine II. A neutron and X-ray diffraction study of $(Mg–Al)^{VI}$ and $(Si–Al)^{IV}$ ordering in monoclinic sapphirine. Contributions to Mineralogy and Petrology, 68, 357–368.

Jamieson, P. B., DeFontaine, D., and Abrahams, S. C. (1969) Determination of atomic ordering arrangements from a study of satellite reflections. Journal of Applied Crystallography, 2, 24–30.

Korekawa, M. (1967) Theorie der Satellitenreflexe. Habilitationsschrift der Ludwig-Maximilians-Universität, München.

McKie, D. (1959) Yoderite, a new hydrous magnesium iron aluminosilicate from Mautia Hill, Tanganyika. Mineralogical Magazine, 32, 282–307.

McKie, D., and Bradshaw, N. (1966) A green variety of yoderite. Nature, 210, 1148.

Nakajima, Y., and Ribbe, P. H. (1981) Twinning and superstructure of Al-rich mullite. American Mineralogist, 66, 142–147.

Ribbe, P. H., Nakajima, Y., and Higgins, J. B. (1981) Modulated structures in mullite and yoderite. Geological Society of America Abstracts with Programs, 13, 537.

Schreyer, W. (1974) Whiteschist, a new type of metamorphic rock formed at high pressures. Geologische Rundschau, 63, 597–609.

Schreyer, W., and Yoder, H. S., Jr. (1966) Yoderite synthesis, stability and interpretation of its natural occurrence. Carnegie Institution of Washington Year Book, 66, 376–380.

Shannon, R. D. (1976) Revised effective ionic radii and systematic studies of interatomic distances in halides and chalcogenides. Acta Crystallographica, A32, 751–767.

Smith, J. V. (1974) Feldspar Minerals, Volume 1. Springer-Verlag, New York.

Vaughn, M. T., and Weidner, D. J. (1978) The relationship of elasticity and crystal structure in andalusite and sillimanite. Physics and Chemistry of Minerals, 3, 133–144.

Winter, J. K., and Ghose, S. (1979) Thermal expansion and high-temperature crystal chemistry of the Al_2SiO_5 polymorphs. American Mineralogist, 64, 573–586.

Manuscript received, June 10, 1981;
accepted for publication, September 25, 1981.